Front. Mater. Sci. 2024, 18(1): 240672
https://doi.org/10.1007/s11706-024-0672-1

RESEARCH ARTICLE

Mesoporous molecular sieve confined phase change materials with high absorption, enhanced thermal conductivity, and cooling energy charging/discharging capacity

Qi Zhang (✉), Chongyang Liu, Xuehong Wu, Xueling Zhang, and Jun Song

School of Energy and Power Engineering, Zhengzhou University of Light Industry, Zhengzhou 450007, China

ABSTRACT: The biggest challenge for organic phase change materials (PCMs) used in cold energy storage is to maintain high heat storage capacity while reducing the leakage risk of PCMs during the phase transition process. This is crucial for expanding their applications in the more demanding cold storage field. In this study, novel form-stable low-temperature composite PCMs are prepared with mesoporous materials, namely SBA-15 and CMK-3 (which are prepared using the template method), as supporting matrices and dodecane as the PCM. Owing to the combined effects of capillary forces within mesoporous materials and interactions among dodecane molecules, both dodecane/SBA-15 and dodecane/CMK-3 exhibit outstanding shape stability and thermal cycling stability even after 200 heating/cooling cycles. In comparison to those of dodecane/SBA-15, dodecane/CMK-3 exhibits superior cold storage performance and higher thermal conductivity. Specifically, the phase transition temperature of dodecane/CMK-3 is −8.81 °C with a latent heat of 122.4 $J \cdot g^{-1}$. Additionally, it has a thermal conductivity of 1.21 $W \cdot m^{-1} \cdot K^{-1}$, which is 9.45 times that of dodecane alone. All these highlight its significant potential for applications in the area of cold energy storage.

KEYWORDS: cold energy storage; phase change material; mesoporous molecular sieve; CMK-3; SBA-15; cooling energy charging/discharging capacity

Contents

Received August 15, 2023; accepted December 10, 2023

E-mail: 1990922zhangqi@zzuli.edu.cn

1 Introduction

In recent years, in response to global climate change and energy crisis, energy conservation and emission reduction have become the general direction of green and low-carbon development worldwide [1–3]. Phase change materials (PCMs) can undergo a phase change process, enabling them to store or release a large amount of latent heat within a certain temperature range, which are mainly divided into organic PCMs and inorganic PCMs [4–5]. Cold energy storage utilizing PCMs has emerged as a crucial energy-saving technology within various application domains, including energy conservation in the built environment, cold storage systems [6–7], thermal management of electronic devices [8–11], and cold chain transportation [12–13]. This technology effectively addresses the challenge of balancing energy supply and demand, thus offering a solution to the energy mismatch issue. In comparison to inorganic PCMs, organic PCMs have garnered significant attention from researchers due to their notable advantages, such as low subcooling, non-corrosive nature, and high stability [14–15]. Nevertheless, practical applications of low-temperature organic PCMs, which are in the liquid state at room temperature, face certain drawbacks such as poor thermal conductivity and susceptibility to leakage. These limitations hinder the wider utilization of low-temperature organic PCMs [16–18]. To address these drawbacks, a promising approach has been proposed to prepare composite PCMs, which involves impregnating or encapsulating PCMs within supporting materials with high thermal conductivity and structural stability.

The encapsulation technique not only increases the thermal conductivity, but also prevents the leakage of liquid PCMs. However, it is important to note that the fabrication process for phase change microcapsules through encapsulation is more intricate and involves higher preparation costs compared to other methods [14]. In contrast to the phase change microcapsule technology, the impregnation method is regarded as a simple and cost-effective manufacturing process [19]. In this approach, porous materials absorb liquid PCMs into their pores, preventing the leakage of PCMs during the phase change process owing to the great capillary forces as a result of the large specific surface area. Based on the endowed chemical inertness as well as other physical and mechanical properties, common porous materials suitable for PCM carriers have been explored, which include expanded graphite [20], foam metals [21–22], expanded perlite [23], metal–organic framework materials (MOFs) [24], and porous polymers [25–26]. Previous studies have found that porous materials such as foam metals (e.g., foam copper) and expanded perlite exhibit poorer reliability in securely retaining PCMs within the carrier due to weak capillary forces in larger pores [27]. Additionally, MOFs and porous polymers have limited chemical stability and are prone to rupture, resulting in a reduced level of widespread attention [28–29]. On the other hand, carbon-based supporting materials such as expanded graphite have emerged as a research hotspot due to their favorable pore structure that helps prevent leakage. Moreover, their structure boasts a high aspect ratio and provides continuous thermal pathways, enabling enhanced thermal conductivity performance. Furthermore, carbon-based support materials have garnered attention for their excellent mechanical properties, chemical stability, and high electrical conductivity [2,30]. Carbon-based materials such as expanded graphite exhibit strong adsorption properties for medium-temperature PCMs in the solid state at room temperature due to their larger pore size, but the encapsulation effect for low-temperature PCMs in the liquid state at room temperature is significantly worse, especially during the actual compaction process, low-temperature PCMs are easy to leak out from the carbon-based materials such as expanded graphite [12,31]. As per the classification provided by the International Union of Pure and Applied Chemistry (IUPAC), porous carbon materials can be classified into

three distinct groups based on their pore size: micropore (particle size < 2 nm), mesopore (2 nm < particle size < 50 nm), and macropore (particle size > 50 nm) [28]. In recent years, mesoporous carbon materials have been used as supporting carriers for composite PCMs due to their ordered pore size distribution, suitable pore diameter, high porosity, and specific surface area, which introduce stronger host–guest interactions and thereby avoid leakage of the PCM. In this regard, Feng et al. [32] employed a melt impregnation technique to encapsulate polyethylene glycol (PEG) within the mesoporous carbon FDU-15. The results indicated that the phase transition temperature and enthalpy of PEG/FDU-15 were 50.45 °C and 81.76 $J \cdot g^{-1}$, respectively. Similarly, Li et al. [33] and Han et al. [34] independently synthesized composite PCMs with phase transition temperatures of 37.54 and 129.8 °C, respectively. These materials were composed of paraffin/high-density polyethylene/carbon nanotubes and decanedioic acid/MCM-41, respectively.

At present, PCMs are widely used in medium-high temperature domains, while there has been relatively limited exploration of the application of molecular sieve-encapsulated liquid organic phase change materials in lower-temperature fields. A new shape-stabilized PCM for cold energy storage in the food cold chain logistics field is reported, which utilizes ice as the PCM and a polyether-based three-dimensional network as the support material. The configuration demonstrates excellent cold retention ability with a phase change temperature of 1.9 °C and a latent heat value of 285.9 $J \cdot g^{-1}$ [35]. Liu et al. [36] used decyl alcohol and lauric acid to prepare eutectic PCMs and expanded graphite as support material to prepare a novel PCM through vacuum adsorption method to meet the requirements of vaccine cold chain transportation. The results demonstrated that at an ambient temperature of 31 °C, the novel PCM with a phase change temperature of 2.08 °C could effectively maintain the cold insulation for approximately 10 h. To adapt to the air-conditioned cold storage system, Zhao et al. [13] prepared a composite PCM of dodecanol-tetradecane/expanded graphite with a melting temperature of 3.45 °C and a melting enthalpy of 197.90 $J \cdot g^{-1}$. Although the low-temperature PCMs based on polymers and expanded graphite show a high latent heat value, the researchers did not assess their mechanical strength or investigate any potential leakage phenomena after heating/cooling cycles. Among mesoporous materials, SBA-15, a silicon-based molecular sieve characterized by its ordered two-dimensional straight pore channels and hexagonal crystal structure, is notable, which often serves as an efficient hard template for preparing other ordered molecular sieve materials. One example is CMK-3, a mesoporous molecular sieve material that belongs to carbon-based materials and possesses an ordered pore system. It exhibits superior properties compared to SBA-15, including higher specific surface area, greater pore volume, excellent chemical stability, mechanical stability, thermal stability, and even higher thermal conductivity. CMK-3 has been utilized for adsorbing medium-temperature PCMs due to its robust capillary forces. For example, both SBA-15 and CMK-3 can include lauric acid (LA), but the unique confinement effect of CMK-3 results in a much higher latent heat of phase transition for LA/CMK-3 compared to LA/SBA-15 [37]. Nevertheless, researchers have not yet explored its utilization for adsorbing low-temperature PCMs.

Due to the small pore size and strong capillary force of CMK-3, it is difficult for low-temperature PCMs to leak out in the liquid state. In this study, SBA-15 was used as a template to prepare mesoporous molecular sieve CMK-3. Then, both SBA-15 and CMK-3 were used to encapsulate liquid low-temperature organic PCM dodecane in the preparation of novel form-stable low-temperature composite PCMs (dodecane/SBA-15 and dodecane/CMK-3) suitable for cold energy storage. Additionally, the microstructure and thermal properties of dodecane/SBA-15 and dodecane/CMK-3 were investigated. The results revealed that both dodecane/SBA-15 and dodecane/CMK-3 show mesoporous microstructure along with good thermal stability and cycling stability. However, it was found that dodecane/CMK-3 demonstrates higher latent heat of phase transition, higher thermal conductivity, and enhanced cold storage performance. These findings highlight its significant potential for utilization in the field of cold storage applications.

2 Experimental

2.1 Materials

Dodecane ($C_{12}H_{26}$, M_n = 170.33, analytical reagent, 98 wt.%) was purchased from Aladdin. SBA-15 (particle size: 6–11 nm, SSA: 550–600 $m^2 \cdot g^{-1}$) was supplied by Nanjing XFNANO Materials Tech Co., Ltd. Furfuryl alcohol ($C_5H_6O_2$, M_n = 98.1, analytical reagent, 98 wt.%) and ethanol (CH_3CH_2OH, M_n = 46.07, analytical reagent,

water ⩽ 3 wt.%) were also obtained from Aladdin.

2.2 Preparation of dodecane/CMK-3 and dodecane/SBA-15

The synthesis of the CMK-3 molecular sieve involved utilizing SBA-15 as the rigid template while employing sugar alcohol as the carbon source. This synthetic method enabled the successful formation of CMK-3 possessing its intended molecular sieve structure and properties. During the synthesis procedure, sugar alcohol was introduced into SBA-15's pores before placing it in an air-tight container within a muffle furnace where it underwent gradual heating from 80 to 150 °C at a rate of 5 °C·min^{-1}. It remained at this temperature for three hours before further reaching up to 300 °C following the same heating rate pattern. Then, the temperature was raised to 850 °C at a heating rate of 5 °C and maintained at a constant temperature for 4 h. This sequence was repeated to ensure the complete carbonation of sugar alcohols within the pores of SBA-15 [38]. The prepared sample was diluted threefold with ethanol, filtered using a circulating water vacuum pump, and then dried to obtain the CMK-3 molecular sieve.

Dodecane was placed in a thermostat at a temperature of 25 °C. Then, CMK-3 and SBA-15 were immersed separately into dodecane for encapsulation, as shown in Fig. 1. After a specific amount of time, the composites were refloated, filtered, and dried to obtain dodecane/CMK-3 and dodecane/SBA-15. Different immersion durations were conducted during the preparation process to evaluate the absorbabilities of CMK-3 and SBA-15.

2.3 Characterizations of PCMs

2.3.1 Microstructure testing of PCMs

The morphologies of SBA-15, CMK-3, and PCM-based materials were observed by transmission electron microscopy (TEM) and scanning electron microscopy (SEM). The surface area (S_{BET}), pore volume (V_{pore}), and pore size (D_{pore}) were tested through the Brunauer–Emmett–Teller (BET) experimental apparatus.

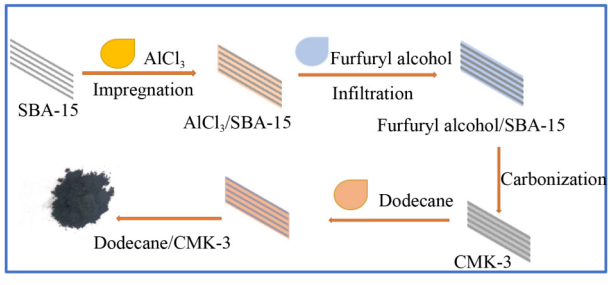

Fig. 1 Preparation of CMK-3 and the PCM of dodecane/CMK-3.

2.3.2 FTIR investigation on PCMs

The structures of PCMs were characterized by Fourier transform infrared spectroscopy (FTIR), the spectra of which were recorded using KBr pellets on a Bruker 550 spectrophotometer from 400 to 4000 cm^{-1}.

2.3.3 Thermal property testing of PCMs

The melting and freezing behaviors of PCMs were measured using a differential scanning calorimetry (DSC). For DSC measurements, 5–8 mg of each sample was sealed in an aluminum pan for characterization at a heating rate of 10 °C·min^{-1} under a constant stream of nitrogen with a flow rate of 50 mL·min^{-1}. The formula for calculating the adsorption ratio of the PCM in the supporting material is as follows:

$$\eta/\% = \frac{\Delta H_{ssPCM}}{\Delta H_{PCM}} \times 100 \quad (1)$$

where ΔH_{ssPCM} refers to the latent heat of the composite shape-stabilized PCMs obtained when the PCM is impregnated with the supporting material, and ΔH_{PCM} also refers to the latent heat of the PCM itself. To confirm the leakage of dodecane in PCMs, high/low temperature alternating wet heat test chambers (THS-250B, China) were used to evaluate their thermal cycling. The heating/cooling cycles were conducted 200 times in the temperature range from −20 to 20 °C, with a heating or cooling rate set at 2 °C·min^{-1}. The thermal stability of PCMs was investigated through thermogravimetric analysis (TGA) using a thermal analyzer (Q600 SDT, TA, URT100). The samples were heated from room temperature to 600 °C at a heating rate of 10 °C·min^{-1} under a nitrogen atmosphere with a flow rate of 100 mL·min^{-1}.

2.3.4 Thermal conductivity testing of PCMs

The PCM was selected for further investigation of thermal conductivity and cooling energy charging/discharging performance. The PCM powders were compressed into a

round block using a homemade cylindrical mold (with an inside diameter of 4 cm and a height of 1 cm) under a pressure of 100 $kg \cdot cm^{-2}$. Based on the volume of the mold we used, we calculated the masses of PCMs needed for fabricating the block with the selected density according to the formula $m = \rho V$. Then, we added the calculated amounts of powders into the mold to fabricate the block. Finally, we measured both the actual volumes and the masses of the formed block to calculate its actual packing density, which was determined to be 771.3 $kg \cdot m^{-3}$. The thermal conductivity of this resulting round block was measured using a thermal constants analyzer (Hot Disk TPS 2500S, Hot Disk AB, Sweden).

2.3.5 Cooling energy charge/discharge performance testing of PCMs

The charging/discharging performance of PCMs was investigated. First, the sample was placed at approximately −20 °C to conduct the cooling energy change process. Then, it was transferred to a room temperature environment for conducting the cooling discharge process. The temperatures of samples during these periods were recorded by a thermal infrared imager (Ti 9, Fluke, ± 0.1 °C).

3 Results and discussion

3.1 Microstructures and FTIR spectra of SBA-15 and CMK-3

The TEM images presented in Fig. 2 depict the molecular sieves SBA-15 and CMK-3. As illustrated in Figs. 2(a) and 2(b), the SBA-15 sample exhibits well-organized striped pores that are parallel to each other, with a tightly arranged and uniform distribution network of pore channels. Moving to Figs. 2(c) and 2(d), it is evident that the surface structure of CMK-3 bears resemblance to that of SBA-15, showcasing distinct ordered porous regions consistent with previous research findings [39–40]. This similarity can be attributed to the fact that CMK-3's structure consists of ordered carbon nanorods initially formed within the pores of the SBA-15 template. Due to the presence of micropores interconnecting the cylindrical channels in SBA-15, these carbon nanorods are firmly connected through these micropores, resulting in smaller carbon nanorods within CMK-3. As a result, CMK-3 has an ordered pore structure similar to that of SBA-15 but with a smaller pore size and enhanced hydrophobicity, rendering it more suitable for the dodecane adsorption [41–42].

To verify the mesoporous structures of SBA-15 and CMK-3, FTIR tests were conducted as illustrated in Fig. 3. In the case of SBA-15, five prominent absorption peaks were observed at specific wavenumbers: 3436, 1630, 1080, 807, and 460 cm^{-1} [43–44]. The absorption peak at 3436 cm^{-1} corresponds to the −OH stretching vibration of the molecular sieve, while the peak at 1630 cm^{-1} represents the stretching vibration of water adsorbed by the molecular sieve. Furthermore, the absorption peaks at 1080, 807, and 460 cm^{-1} can be attributed to the asymmetric stretching vibration, symmetric stretching vibration, and bending vibration of Si−O−Si within the molecular sieve framework. On the other hand, the FTIR analysis of the CMK-3 sample reveals distinctive bands associated with the carbon structure vibrations that distinguish it from SBA-15. Specifically, the absorption peak at 1565 cm^{-1} corresponds to the stretching vibration of aromatic carbon double bonds (C=C), while the band centered at 1130 cm^{-1} is attributed to the tangential motion of C−C bonds in the molecular sieve backbone. The relatively weak absorption band detected at 3436 cm^{-1} can be attributed to both stretching and deformation vibrations of O−H, which are assigned to the phenol group [45]. Additionally, vibrations originating from the Si−O bonds of the residual hard template SBA-15 can be observed in the CMK-3 sample within the wavenumber range of 500 to 900 cm^{-1}. Consequently, both the FTIR results and the TEM images confirm that CMK-3 possesses a similar pore structure to that of SBA-15. Furthermore, these findings validate that no chemical transformations occur during the synthesis of CMK-3 utilizing SBA-15 as a hard template, aligning with previous scientific studies establishing CMK-3 as a reverse replica of SBA-15.

3.2 Absorption capacities of SBA-15 and CMK-3

Hydrophobicity plays a crucial role in the performance of cold storage [46–47]. As shown in Fig. 4(a), SBA-15, which acts as a molecular sieve, possesses a certain level of hydrophilicity that is not conducive to the adsorption of organic PCMs. In contrast, CMK-3, as the inverse replica of SBA-15, exhibits strong hydrophobic properties [48]. The morphology of water droplets on the surface of

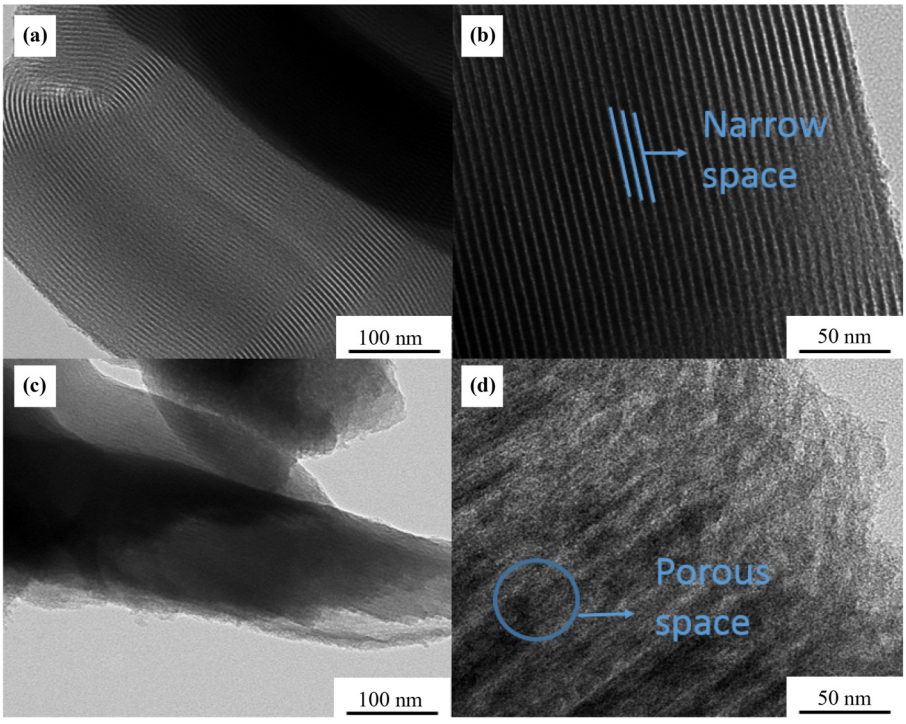

Fig. 2 TEM images of (**a**)(**b**) SBA-15 and (**c**)(**d**) CMK-3.

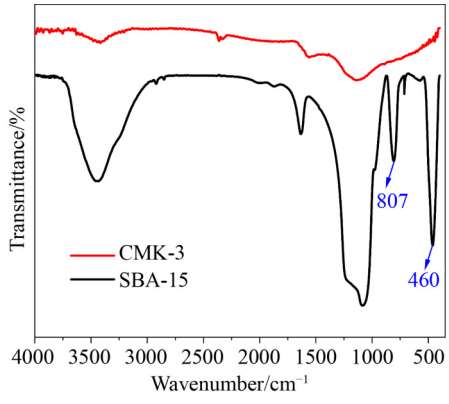

Fig. 3 FTIR spectra of SBA-15 and CMK-3.

CMK-3 is observed in Fig. 4(b), where the hydrophobic angle of CMK-3 was measured to be 143.7°, showing strong hydrophobicity. Furthermore, we evaluated the N_2 adsorption/desorption isotherms and pore size distributions of SBA-15 and CMK-3. Figure 4(c) illustrates the N_2 adsorption/desorption isotherms of the samples, which exhibit typical type IV isotherms and pronounced hysteresis loops. This behavior indicates the presence of an ordered mesoporous pore structure in the samples [49–50]. As shown in Fig. 4(d), the specific surface area, pore volume, and average pore size of the samples were calculated by employing the Brunauer–Emmett–Teller (BET) and Barrett–Joyner–Halenda (BJH) equations. It is noteworthy that CMK-3 has a significantly larger surface area than that of SBA-15 due to the presence of disordered micropores resulting from the precursor carbonation [51]. Specifically, the specific surface areas of CMK-3 and SBA-15 are determined to be 1164.61 and 560 $cm^2 \cdot g^{-1}$, respectively. The corresponding pore volumes for CMK-3 and SBA-15 are 1.45 and 0.38 $cm^3 \cdot g^{-1}$, respectively. Additionally, the average pore sizes are measured to be 2.05 nm for CMK-3 and 5.8 nm for SBA-15, as shown in Table 1. These findings indicate that CMK-3 possesses a larger specific surface area compared to that of SBA-15. Furthermore, CMK-3 exhibits a higher pore volume and a smaller pore size per unit mass, making it more suitable as a support material for encapsulated PCMs.

Figure 5 presents the results of adsorption time tests conducted to evaluate the adsorption performance of SBA-15 and CMK-3. DSC analysis was employed to determine the mass fractions of dodecane adsorbed by each material at different adsorption times. The adsorption ratio of dodecane/SBA-15 and dodecane/CMK-3 composite PCMs compared to pure dodecane was used for the calculation of these mass fractions. In Fig. 5, it is evident that the mass fraction of adsorbed dodecane increases as the adsorption time progresses. For SBA-15,

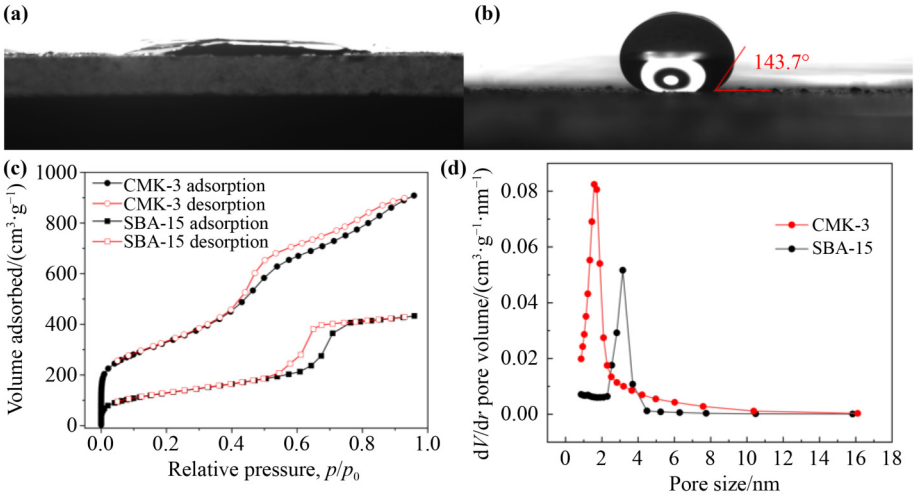

Fig. 4 Hydrophilic/hydrophobic performances of (**a**) SBA-15 and (**b**) CMK-3. (**c**) N_2 adsorption/desorption isotherms and (**d**) pore size distributions of SBA-15 and CMK-3.

Table 1 Physical properties of SBA-15 and CMK-3

Sample	Physical properties			
	Surface performance	Surface area/($cm^2 \cdot g^{-1}$)	Average pore size/nm	Pore volume/($cm^3 \cdot g^{-1}$)
SBA-15	hydrophilic	560	5.8	0.38
CMK-3	hydrophobic	1164.61	2.05	1.45

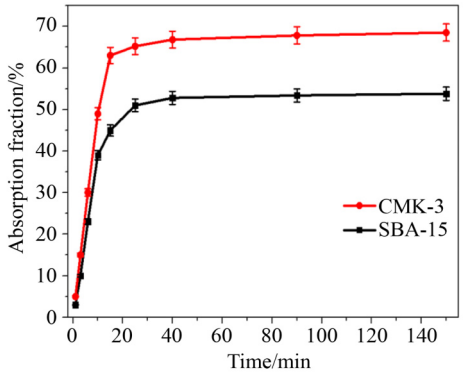

Fig. 5 Absorption fraction–time curves of SBA-15 and CMK-3.

the mass fraction of dodecane rapidly increases from 0 to 39% within the first 10 min. Subsequently, the increase becomes more gradual and eventually reaches 52.8% after 40 min. Similarly, the absorption capacity of CMK-3 increased by 66.8%, indicating a higher adsorption ratio compared to SBA-15. The results indicate that CMK-3 possesses approximately a 21% higher adsorption capacity than that of SBA-15, with CMK-3 achieving an adsorption capacity exceeding 70% [51].

3.3 Microstructures and FTIR spectra of dodecane/SBA-15 and dodecane/CMK-3

The SEM images in Fig. 6 depict the morphologies of dodecane/SBA-15 and dodecane/CMK-3. In Figs. 6(a) and 6(b), it is evident that dodecane/SBA-15 exhibits a "German sausage" structure similar to that of SBA-15, with well-defined mesoporous channels observable on the surface, indicating that encapsulating the PCM within the molecular sieve does not alter its inherent morphology [51]. Furthermore, Figs. 6(c) and 6(d) illustrate that the dodecane/CMK-3 sample exhibits a similar morphological structure to that of the dodecane/SBA-15 sample, characterized by a significant number of ordered strip pore structures. This similarity can be attributed to CMK-3 being synthesized using SBA-15 as a template and inheriting its characteristic ordered mesoporous channels.

To further analyze the microstructures of dodecane/SBA-15 and dodecane/CMK-3, Fig. 7 presents the FTIR spectra of dodecane, SBA-15, CMK-3, as well as dodecane/SBA-15 and dodecane/CMK-3. In the FTIR spectra of dodecane, the peaks observed at 2958, 2925, and 2855 cm^{-1} correspond to the stretching vibrations of the aliphatic chain C−H. The absorption peaks at 1467

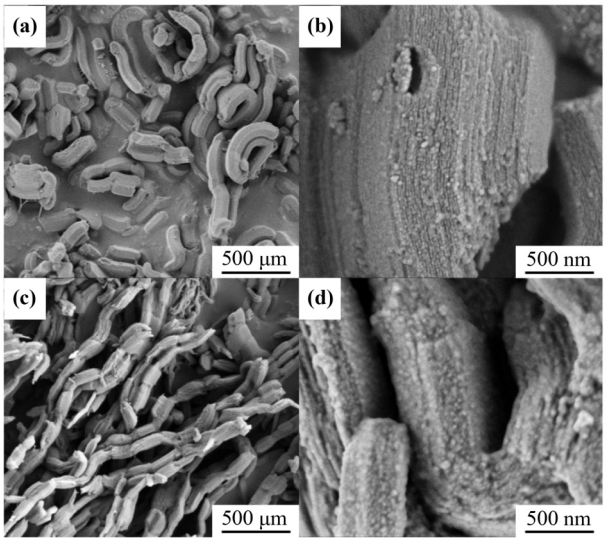

Fig. 6 SEM images of (**a**)(**b**) dodecane/SBA-15 and (**c**)(**d**) dodecane/CMK-3.

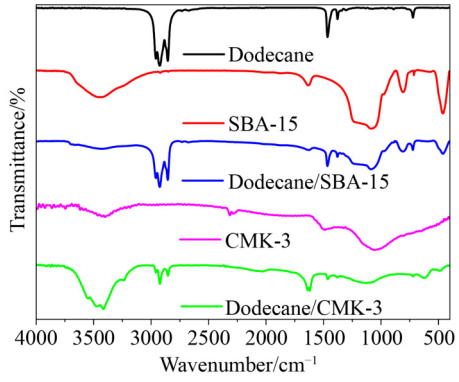

Fig. 7 FTIR spectra of dodecane, SBA-15, CMK-3, dodecane/SBA-15 and dodecane/CMK-3.

and 1378 cm^{-1} are attributed to the bending vibrations of the $-CH_3$ group and $-CH_2$ group C–H, respectively. Additionally, the absorption peak at 722 cm^{-1} arises from the in-plane wobbling vibrations of more than four consecutive $-CH_2$ groups [52–53]. The FTIR spectra of both dodecane/SBA-15 and dodecane/CMK-3 composite PCMs exhibit characteristic absorption peaks from both the PCM and support materials without any new absorption peaks observed. This observation confirms that there is a physical interaction between dodecane and the support materials.

3.4 Melting/freezing behaviors and thermal stability of dodecane/SBA-15 and dodecane/CMK-3

In Fig. 8(a), the DSC curves of dodecane/SBA-15 and dodecane/CMK-3 closely resemble those of pure dodecane. Pure dodecane exhibits a melting temperature of −9.68 °C and a melting enthalpy of 179.34 $J \cdot g^{-1}$. The cooling temperature is −12.32 °C, while the solidification enthalpy is 176.24 $J \cdot g^{-1}$. When compounded with molecular sieves, the thermophysical properties of dodecane remain largely unchanged. Specifically, the melting and solidification enthalpy of dodecane/CMK-3 is 122.4 and 119.6 $J \cdot g^{-1}$, respectively, while the melting and cooling temperature is −8.81 and −11.86 °C, respectively. On the other hand, dodecane/SBA-15 displays a melting enthalpy and solidification enthalpy of 94.2 and 93.9 $J \cdot g^{-1}$, respectively, with melting and cooling temperatures as −8.87 and −11.82°C. The encapsulation ratio of dodecane in dodecane/SBA-15 and dodecane/CMK-3 composite PCMs are calculated by comparing the melting enthalpy of the composite PCM to that of pure dodecane, resulting in encapsulation ratio of 52.5% and 68.25%, respectively. It is noteworthy that the composite PCM of dodecane/CMK-3 exhibits a bimodal crystallization phenomenon different from that of pure dodecane during the phase change process. This difference can be attributed to both the homogeneous nucleation process and heterogeneous nucleation process occurring in dodecane impregnated with CMK-3, as well as the strong interactions between the CMK-3's skeleton and dodecane's molecules which influence their regular arrangement, resulting in the appearance of this bimodal phenomenon [54–57]. To evaluate the thermal stability, the TGA method was employed to analyze the weight loss curves, as depicted in Fig. 8(b). Dodecane starts losing weight at approximately 28.75 °C and reaches maximum mass loss at 171 °C, leaving only about 3% of the initial mass. Molecular sieves SBA-15 and CMK-3 demonstrate excellent thermal stability as they do not exhibit any significant weight loss until reaching 600 °C. Specifically, SBA-15 experiences a maximum weight loss of approximately 3%, while CMK-3 shows about 2% weight reduction. Consequently, the presence of these molecular sieves significantly reduces the maximum weight loss of dodecane in both dodecane/SBA-15 and dodecane/CMK-3 systems compared to pure dodecane alone. The residual weights for these mixtures are recorded at 48.25% and 32.12%, respectively, because 51.75% and 67.88% of dodecane adsorbed by SBA-15 and CMK-3, respectively, are decomposed at high temperatures. These findings are consistent with the results obtained from the DSC tests. The TGA results demonstrate that the thermal

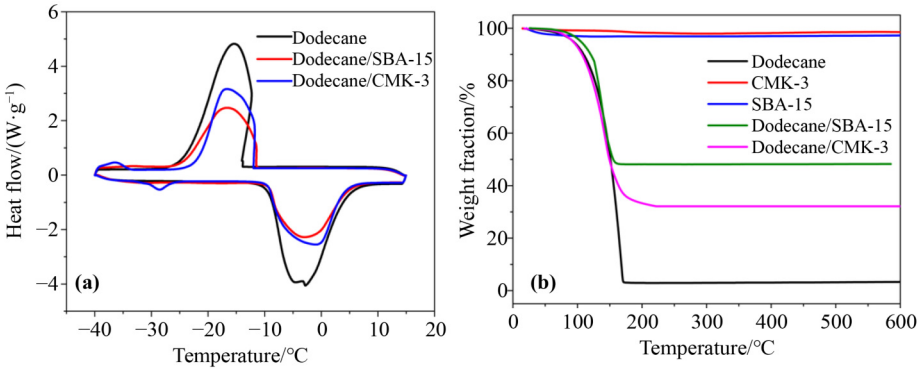

Fig. 8 The melting and freezing behaviors of dodecane/SBA-15 and dodecane/CMK-3: (**a**) DSC curves; (**b**) TGA curves.

stability of dodecane is improved when it is encapsulated in SBA-15 and CMK-3. Overall, the combination of DSC and TGA analysis reveals that dodecane/SBA-15 and dodecane/CMK-3 have great cold energy storage capacity and thermal stability.

3.5 Reversible stability of dodecane/SBA-15 and dodecane/CMK-3

The microstructure, reversible stability and leakage phenomenon of dodecane/SBA-15 and dodecane/CMK-3 were tested after 200 heating/cooling cycles, as depicted in Fig. 9. It can be seen that there were no significant changes in the morphological structures of both dodecane/SBA-15 and dodecane/CMK-3 composite PCMs. In Figs. 9(c)–9(f), it can be observed that there is no leakage of dodecane/CMK-3 before and after the heating/cooling cycles due to the adherence of its outer layer to adheres tightly the mesoporous wall, which reduces its mobility. Despite experiencing a slight decrease in phase-change latent heat for both composite PCMs (dodecane/SBA-15 and dodecane/CMK-3), this loss is negligible. Specifically, after undergoing 200 heating/cooling cycles, the melting enthalpy and solidification enthalpy of dodecane/SBA-15 were 93.8 and 93.2 $J \cdot g^{-1}$, respectively, while those of dodecane/CMK-3 were 121.7 and 118.9 $J \cdot g^{-1}$, respectively. The relative deviations of the melting and solidification enthalpy before the heating/cooling cycles were less than 0.6%. It indicated that the molecular sieves SBA-15 and CMK-3 effectively encapsulate dodecane, preventing its leakage from the mesopores of the support material during the phase change process. All the results show that dodecane/CMK-3 has greater advantages in cold energy storage while ensuring reversible stability.

3.6 Thermal conductivity of dodecane/SBA-15 and dodecane/CMK-3

Figure 10 illustrates results from the thermal conductivity measurements of dodecane, dodecane/SBA-15, and dodecane/CMK-3. The thermal conductivity values of dodecane, dodecane/SBA-15, and dodecane/CMK-3 were found to be 0.128, 0.183, and 1.21 $W \cdot m^{-1} \cdot K^{-1}$, respectively. A comparison with pure dodecane reveals that both dodecane/SBA-15 and dodecane/CMK-3 exhibit significant improvements in thermal conductivity. Particularly, the thermal conductivity of dodecane/CMK-3 is remarkably higher, 9.45 times that of dodecane and 561% that of dodecane/SBA-15. These results indicate that SBA-15 and CMK-3, as support materials, are highly effective in enhancing the thermal conductivity of composite PCMs. Additionally, CMK-3 demonstrates superior effectiveness in enhancing the thermal conductivity than SBA-15.

3.7 Cooling energy charging/discharging performance of dodecane/SBA-15 and dodecane/CMK-3

The cooling energy charging/discharging performance of the composite PCM is illustrated in Fig. 11. In Fig. 11(a), it takes 274 s for dodecane/SBA-15 to decrease the temperature from 20 to −5 °C in a low-temperature environment. Subsequently, dodecane/SBA-15 shows 355 s of cool temperature platforms. dodecane/CMK-3 only takes 96 s to decrease from 20 to −5 °C and exhibits 132 s of cool temperature platforms. On the other hand, It takes 195 s for dodecane/SBA-15 to increase from −20 to −9 °C, and then it shows 317 s of cool temperature platforms between −9 and −4.27 °C. In contrast, dodecane/CMK-3 only needs 72 s to raise the temperature

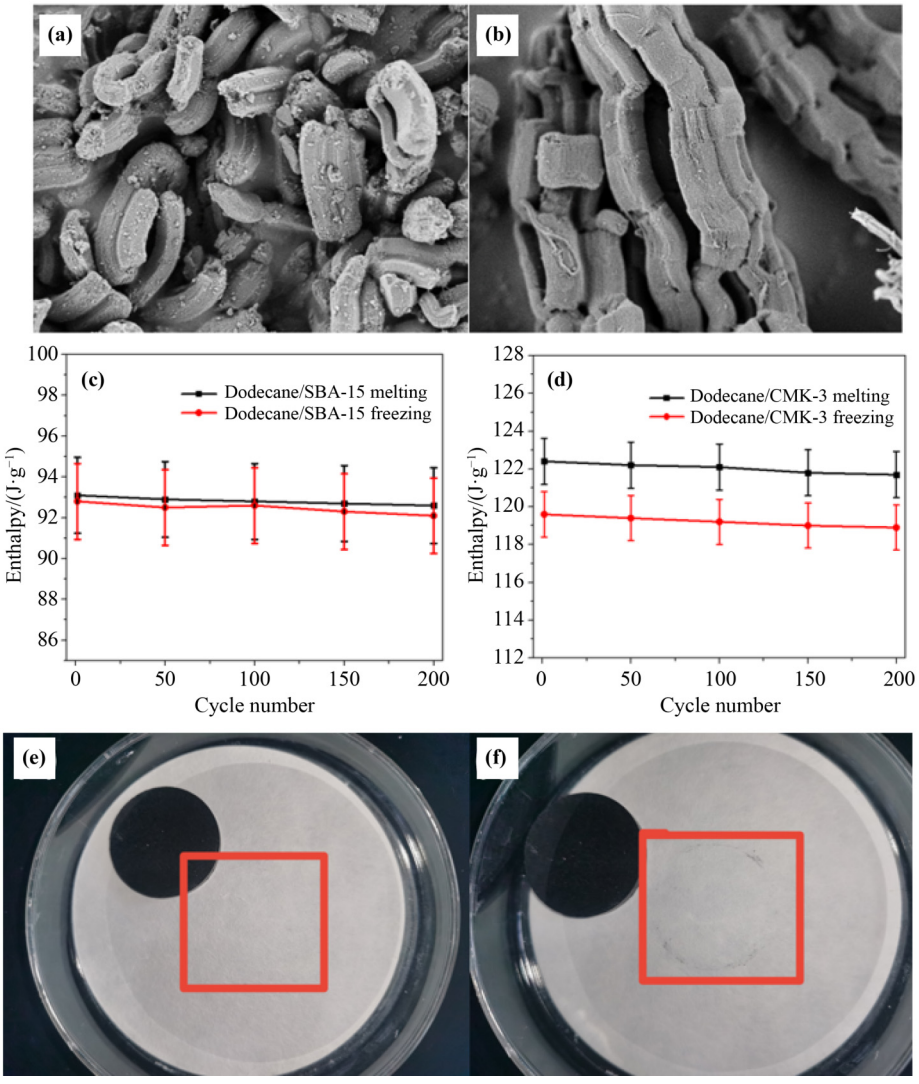

Fig. 9 SEM images of (**a**) dodecane/SBA-15 and (**b**) dodecane/CMK-3. Melting and freezing enthalpy of (**c**) dodecane/SBA-15 and (**d**) dodecane/CMK-3 with different heating/cooling cycles. Leakages of dodecane/CMK-3 samples (**e**) before and (**f**) after heating/cooling cycles.

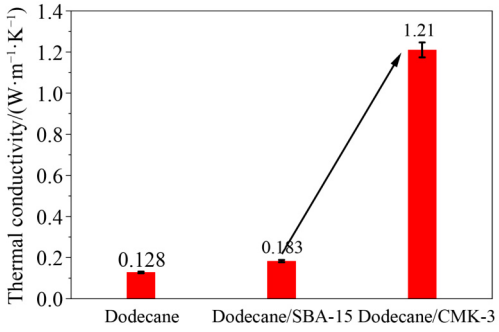

Fig. 10 Thermal conductivities of dodecane/SBA-15 and dodecane/CMK-3 compared with that of dodecane.

from −20 to −9 °C, with 113 s of cool temperature platforms between −9 and −4.27 °C. Comparing the two composite PCMs, dodecane/CMK-3 exhibits a significant advantage in terms of cooling energy charging/discharging performance. This improvement can be attributed to the higher thermal conductivity of dodecane/CMK-3, which enables faster release or storage of cooling energy. To further evaluate the cold storage performance of dodecane/SBA-15 and dodecane/CMK-3, the thermal charging capacity of the PCM was calculated according to the following equation:

$$Q_T = \int_{-9}^{-4.27} C_p \mathrm{d}T + \Delta H_m \tag{2}$$

where Q_T is the heat storage capacity of the PCM, T is the Celsius temperature of the PCM, C_p is the specific heat capacity of the PCM, and ΔH_m is the latent heat value of

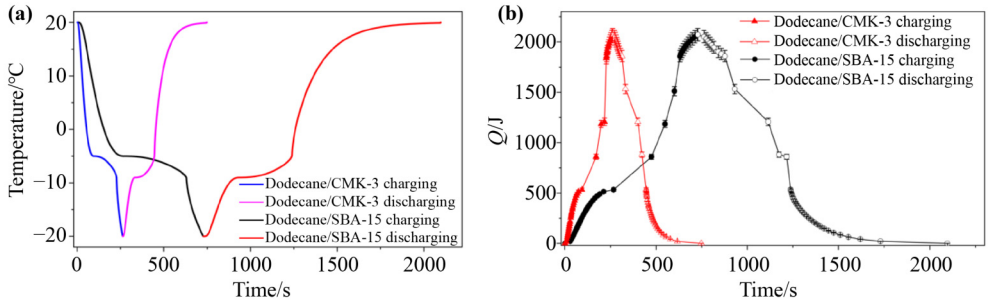

Fig. 11 (**a**) Temperature and (**b**) cooling thermal charging/discharging behaviors of dodecane/SBA-15 and dodecane/CMK-3 in the cooling and heating process.

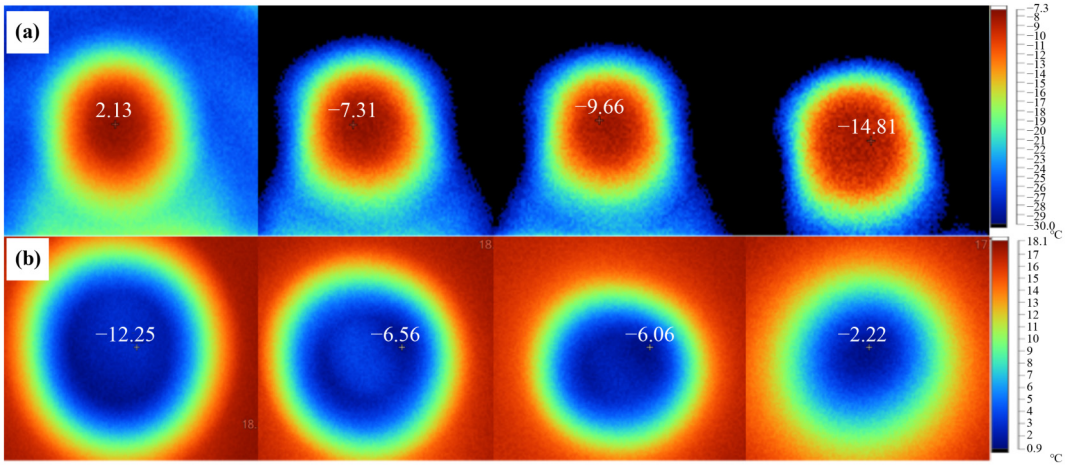

Fig. 12 Infrared images of dodecane/CMK-3 in (**a**) cooling and (**b**) heating processes.

the PCM. In Fig. 11(b), it can be observed that the thermal charging characteristics of dodecane/CMK-3 demonstrate a rapid increase to 2071 J within 263 s. On the other hand, it takes 729 s for dodecane/SBA-15 to reach the same level of heat storage capacity, which indicates a duration that is approximately 2.77 times longer than that required by dodecane/CMK-3. As a result, it can be concluded that dodecane/CMK-3 exhibits superior cold storage capabilities and an effective heat storage capacity.

The formable dodecane/CMK-3 composite PCM consists of 66.8% dodecane and has a density of 771.3 kg·m^{-3}. The surface temperature variation of the dodecane/CMK-3 sample was recorded using an infrared thermal camera to investigate its effectiveness in cooling energy charging/discharging process, as shown in Fig. 12. It is evident that during cooling energy charging stage, there is a rapid decrease in temperature of the composite PCM to −7.31 °C within 206 s, followed by temperature platforms at about −10 °C for 229 s. The decrease rate of the temperature in this process slows down compared to the initial drop due to the thermal enthalpy of dodecane/CMK-3. The dodecane/CMK-3 sample can maintain a temperature below −2 °C for over 200 s at room temperature. Furthermore, it exhibiteds 113 s of cool temperature platforms. These results are consistent with conclusions in Fig. 11(a) and demonstrate that dodecane/CMK-3 has excellent performance in cold storage, holding significant potential in various fields such as cold chain transportation, temperature sensors, aerospace applications, and low-temperature waste heat recovery.

4 Conclusion

In this study, the form-stable low-temperature composite PCM for cold energy storage was synthesized using molecular sieves as the supporting materials and dodecane as the PCM. The latent heats of dodecane/CMK-3 and dodecane/SBA-15 are 122.4 and 94.2 J·g^{-1}, with the phase transition temperatures of −8.81 and −8.87 °C, respectively. It is noteworthy that no leakage is observed

after 200 heating/cooling cycles for both form-stable low-temperature composite PCMs. The thermal conductivity of dodecane/CMK-3 is measured at 1.21 $W \cdot m^{-1} \cdot K^{-1}$, which is 9.45 times that of dodecane due to the higher thermal conductivity of CMK-3 compared to that of SBA-15. Moreover, the cooling energy charging/discharging performance of dodecane/CMK-3 is nearly three times faster than that of dodecane/SBA-15, indicating superior cold storage performance. These results highlight the suitability of molecular sieve CMK-3, compared to SBA-15, as a supporting matrix for liquid low-temperature organic PCMs. Dodecane/CMK-3 exhibits significant potential for applications in cold energy storage, such as cold chain transportation, temperature sensors, aerospace clothing, and low-temperature waste heat recovery fields.

Declaration of competing interests The authors declare that they have no competing interests.

Acknowledgements This work was supported by the National Natural Science Foundation of China (Grant No. 51906230), the Key scientific and technological projects in Henan Province (Grant No. 212102210007), and the Project of Zhongyuan Science and Technology Innovation Talents (Grant No. 234200510011).

References

[1] Yang Y, Liu S, Zhang G, et al. Cellulose nanofiber encapsulated polyethylene glycol phase change composites containing AIE-gen for monitoring leak process. Composites Part A: Applied Science and Manufacturing, 2023, 167: 107452

[2] Selvnes H, Allouche Y, Manescu R I, et al. Review on cold thermal energy storage applied to refrigeration systems using phase change materials. Thermal Science and Engineering Progress, 2021, 22: 100807

[3] Yu K, Liu Y, Yang Y. Review on form-stable inorganic hydrated salt phase change materials: preparation, characterization and effect on the thermophysical properties. Applied Energy, 2021, 292: 116845

[4] Li X, Sheng X, Fang Y, et al. Wearable Janus-type film with integrated all-season active/passive thermal management, thermal camouflage, and ultra-high electromagnetic shielding efficiency tunable by origami process. Advanced Functional Materials, 2023, 33(18): 2212776

[5] Liu S, Quan B, Sheng M, et al. A novel *in-situ* growth ZIF-67 on biological porous carbon encapsulated phase change composites with electromagnetic interference shielding and multifunctional energy conversion. Nano Energy, 2023, 114: 108669

[6] Karthikeyan K, Mariappan V, Anish R, et al. Experimental study on the charging and discharging behaviour of capric–lauric acid/oleic acid mixture in a cold thermal energy storage system for cold storage applications. Materials Today: Proceedings, 2021, 46(Part 19): 10022–10029

[7] Li Y, Zhang X, Munyalo J M, et al. Preparation and thermophysical properties of low temperature composite phase change material octanoic–lauric acid/expanded graphite. Journal of Molecular Liquids, 2019, 277: 577–583

[8] Quan B, Wang M, Hu X, et al. Large-scale fabrication of flexible EVA/EG@PW phase change composites with high thermal conductivity for thermal management. Macromolecular Materials and Engineering, 2023, 308(9): 2300036

[9] Hu X, Huang X, Quan B, et al. Tree-inspired and scalable high thermal conductivity ethylene–vinyl acetate copolymer/expanded graphite/paraffin wax phase change composites for efficient thermal management. Chemical Engineering Journal, 2023, 471: 144720

[10] Peng J, Deng C, Wei F, et al. A hybrid thermal management system combining liquid cooling and phase change material for downhole electronics. Journal of Energy Storage, 2023, 72: 108610

[11] Peng J, Lan W, Wei F, et al. A numerical model coupling multiple heat transfer modes to develop a passive thermal management system for logging tool. Applied Thermal Engineering, 2023, 223: 120011

[12] Zhao L, Li M, Yu Q, et al. Improving the thermal performance of novel low-temperature phase change materials through the configuration of 1-dodecanol-tetradecane nanofluids/expanded graphite composites. Journal of Molecular Liquids, 2021, 322: 114948

[13] Zhao L, Yu Q, Li M, et al. Preparation and thermal properties of low-temperature composite phase-change materials based on a binary eutectic mixture with expanded graphite: effect of particle size and mass fraction. Journal of Energy Storage, 2021, 40: 102778

[14] Nie B, Palacios A, Zou B, et al. Review on phase change materials for cold thermal energy storage applications. Renewable & Sustainable Energy Reviews, 2020, 134: 110340

[15] Konuklu Y, Erzïn F, Akar H B, et al. Cellulose-based myristic acid composites for thermal energy storage applications. Solar Energy Materials and Solar Cells, 2019, 193: 85–91

[16] Zhang X, Shi Q, Luo L, et al. Research progress on the phase change materials for cold thermal energy storage. Energies, 2021, 14(24): 8233

[17] Hameed G, Ghafoor M A, Yousaf M, et al. Low temperature phase change materials for thermal energy storage: current status and computational perspectives. Sustainable Energy Technologies and Assessments, 2022, 50: 101808

[18] Jafaripour M, Sadrameli S M, Mousavi S A H S, et al. Experimental investigation for the thermal management of a coaxial electrical cable system using a form-stable low temperature phase change material. Journal of Energy Storage, 2021, 44(B): 103450

[19] Shen Z, Kwon S, Lae H L, et al. Preparation and application of composite phase change materials stabilized by cellulose nanofibril-based foams for thermal energy storage. International Journal of Biological Macromolecules, 2022, 222(B): 3001–3013

[20] Zhang Q, Wang H, Ling Z, et al. RT100/expand graphite composite phase change material with excellent structure stability, photo-thermal performance and good thermal reliability. Solar Energy Materials and Solar Cells, 2015, 140: 158–166

[21] Li W Q, Guo S J, Tan L, et al. Heat transfer enhancement of nano-encapsulated phase change material (NEPCM) using metal foam for thermal energy storage. International Journal of Heat and Mass Transfer, 2021, 166: 120737

[22] Zhao S, Li J, Wu Y, et al. Porous titanium dioxide foams: a promising carrier material for medium- and high-temperature thermal energy storage. Energy & Fuels, 2020, 34(7): 8884–8890

[23] Bian Y, Wang K, Wang J, et al. Preparation and properties of capric acid: stearic acid/hydrophobic expanded perlite-aerogel composite phase change materials. Renewable Energy, 2021, 179: 1027–1035

[24] Luan Y, Yang M, Ma Q, et al. Introduction of an organic acid phase changing material into metal–organic frameworks and the study of its thermal properties. Journal of Materials Chemistry A: Materials for Energy and Sustainability, 2016, 4(20): 7641–7649

[25] Tang J, Yang M, Yu F, et al. 1-Octadecanol@hierarchical porous polymer composite as a novel shape-stability phase change material for latent heat thermal energy storage. Applied Energy, 2017, 187: 514–522

[26] Musiał M, Lichołai L, Katunský D. Modern thermal energy storage systems dedicated to autonomous buildings. Energies, 2023, 16(11): 4442

[27] Feng D, Feng Y, Qiu L, et al. Review on nanoporous composite phase change materials: fabrication, characterization, enhancement and molecular simulation. Renewable & Sustainable Energy Reviews, 2019, 109: 578–605

[28] Pérez-Mayoral E, Matos I, Bernardo M, et al. New and advanced porous carbon materials in fine chemical synthesis. Emerging precursors of porous carbons. Catalysts, 2019, 9(2): 133

[29] Notario B, Pinto J, Rodriguez-Perez M A. Nanoporous polymeric materials: a new class of materials with enhanced properties. Progress in Materials Science, 2016, 78–79: 93–139

[30] Li H, Hu C, He Y, et al. Emerging surface strategies for porous materials-based phase change composites. Matter, 2022, 5(10): 3225–3259

[31] Yu X K, Tao Y B. Preparation and characterization of paraffin/expanded graphite composite phase change materials with high thermal conductivity. International Journal of Heat and Mass Transfer, 2022, 198: 123433

[32] Feng D, Li P, Feng Y, et al. Using mesoporous carbon to pack polyethylene glycol as a shape-stabilized phase change material with excellent energy storage capacity and thermal conductivity. Microporous and Mesoporous Materials, 2021, 310: 110631

[33] Li X, Sheng X, Guo Y, et al. Multifunctional HDPE/CNTs/PW composite phase change materials with excellent thermal and electrical conductivities. Journal of Materials Science & Technology, 2021, 86: 171–179

[34] Han L, Ma G, Xie S, et al. Preparation and characterization of the shape-stabilized phase change material based on sebacic acid and mesoporous MCM-41. Journal of Thermal Analysis and Calorimetry, 2017, 130(2): 935–941

[35] Zhang Y, Xu Y, Lu R, et al. Form-stable cold storage phase change materials with durable cold insulation for cold chain logistics of food. Postharvest Biology and Technology, 2023, 203: 112409

[36] Liu L, Zhang X, Xu X, et al. Development of low-temperature eutectic phase change material with expanded graphite for vaccine cold chain logistics. Renewable Energy, 2021, 179: 2348–2358

[37] Kadoono T, Ogura M. Heat storage properties of organic phase-change materials confined in the nanospace of mesoporous SBA-15 and CMK-3. Physical Chemistry Chemical Physics, 2014, 16(12): 5495–5498

[38] Lu A H, Schmidt W, Taguchi A, et al. Taking nanocasting one step further: replicating CMK-3 as a silica material. Angewandte Chemie International Edition, 2002, 41(18): 3489–3492

[39] Shivudu G, Khan S, Chandraraj K, et al. Immobilization of recombinant endo-1,4-β-xylanase on ordered mesoporous matrices for xylooligosaccharides production. ChemistrySelect, 2019, 4(38): 11214–11221

[40] He J, Ma K, Jin J, et al. Preparation and characterization of octyl-modified ordered mesoporous carbon CMK-3 for phenol adsorption. Microporous and Mesoporous Materials, 2009, 121(1–3): 173–177

[41] Vinu A, Hossain K Z, Satish Kumar G, et al. Adsorption of l-histidine over mesoporous carbon molecular sieves. Carbon, 2006, 44(3): 530–536

[42] Zhou L, Liu X, Li J, et al. Synthesis of ordered mesoporous carbon molecular sieve and its adsorption capacity for H_2, N_2,

O_2, CH_4 and CO_2. Chemical Physics Letters, 2005, 413(1–3): 6–9

[43] Mohammadi Ziarani G, Badiei A, Mousavi S, et al. Application of amino-functionalized SBA-15 type mesoporous silica in one-pot synthesis of spirooxindoles. Chinese Journal of Catalysis, 2012, 33(11–12): 1832–1839

[44] Shahbazi A, Younesi H, Badiei A. Functionalized SBA-15 mesoporous silica by melamine-based dendrimer amines for adsorptive characteristics of Pb(II), Cu(II) and Cd(II) heavy metal ions in batch and fixed bed column. Chemical Engineering Journal, 2011, 168(2): 505–518

[45] Gaspar H, Andrade M, Pereira C, et al. Alkene epoxidation by manganese(III) complexes immobilized onto nanostructured carbon CMK-3. Catalysis Today, 2013, 203: 103–110

[46] Pu L, Liu R, Huang H, et al. Experimental study of cyclic frosting and defrosting on microchannel heat exchangers with different coatings. Energy and Buildings, 2020, 226: 110382

[47] Yang K S, Lu W, Wu Y L. Visualization of patterned modified surfaces in condensation and frosting states. Energies, 2019, 12(23): 4471

[48] Li X, Ma Y, Zuo Y, et al. The efficient enrichment of marine peptides from the protein hydrolysate of the marine worm *Urechis unicinctus* by using mesoporous materials MCM-41, SBA-15 and CMK-3. Analytical Methods, 2021, 13(21): 2405–2414

[49] Liu Y, Li Z, Yang X, et al. Performance of mesoporous silicas (MCM-41 and SBA-15) and carbon (CMK-3) in the removal of gas-phase naphthalene: adsorption capacity, rate and regenerability. RSC Advances, 2016, 6(25): 21193–21203

[50] Wang Q, Wang Z, Zheng T, et al. Size control of SBA-15 by tuning the stirring speed for the formation of CMK-3 with distinct adsorption performance. Nano Research, 2016, 9(8): 2294–2302

[51] Chen Y, Liu C, Situ Y, et al. Enhancing thermal conductivity and photo-driven thermal energy charging/discharging rate of annealed CMK-3 based phase change material. Nanomaterials, 2019, 9(3): 364

[52] Song Y, Zhang N, Jing Y, et al. Experimental and numerical investigation on dodecane/expanded graphite shape-stabilized phase change material for cold energy storage. Energy, 2019, 189: 116175

[53] Zhu K, Qi H, Wang S, et al. Preparation and characterization of melamine-formaldehyde resin micro- and nanocapsules filled with n-dodecane. Journal of Macromolecular Science Part B: Physics, 2012, 51(10): 1976–1990

[54] Hekimoğlu G, Sarı A, Gencel O, et al. Thermal energy storage characteristics of polyacrylic acid/dodecanol/carbon nanofiber composites as thermal conductive shape-stabilized composite phase change materials. International Journal of Energy Research, 2022, 46(14): 20873–20885

[55] Zhang X X, Fan Y F, Tao X M, et al. Crystallization and prevention of supercooling of microencapsulated n-alkanes. Journal of Colloid and Interface Science, 2005, 281(2): 299–306

[56] Qian Z, Shen H, Fang X, et al. Phase change materials of paraffin in h-BN porous scaffolds with enhanced thermal conductivity and form stability. Energy and Buildings, 2018, 158: 1184–1188

[57] Pan X, Zhang N, Yuan Y, et al. Balsa-based porous carbon composite phase change material with photo-thermal conversion performance for thermal energy storage. Solar Energy, 2021, 230: 269–277